Correlation length, finite-geometry effects, and universality in pressurized superfluid helium near T_λ

Gary G. Ihas* and F. Pobell

Institut für Festkörperforschung, Kernforschungsanlage, 517 Jülich, West Germany

(Received 27 September 1973)

The onset temperature $T_0(P)$ for superfluidity of ^{4}He has been measured in $d = 0.1$-, 0.2-, 0.4-, and 0.6-μm wide channels at pressures between saturated vapor pressure and the melting curve. The onset was detected by observing the vanishing of second sound in resonators equipped with superleak transducers. In the channels used the onset temperature $T_0(P)$ was depressed below the bulk transition temperature $T_\lambda(P)$ by $2 \times 10^{-5} \le \epsilon_0 \le 2 \times 10^{-4}$. Here $\epsilon_0 = 1 - T_0(P)/T_\lambda(P)$. For constant d, we find that ϵ_0 is independent of pressure to within our resolution of $\pm 2\%$. From the data the exponent λ' and the coefficient d^* for the equation $\epsilon_0 = (d/d^*)^{-\lambda'}$, and the exponent and coefficient for the correlation length, $\xi = \xi^* \epsilon^{-\nu'}$, have been calculated. We show that λ' and d^*, as well as ν' and ξ^*, and the quantity $\xi \rho_s / T$ are independent of pressure, within our resolution of $\pm 2\%$. The lack of a pressure dependence of the critical exponents is in agreement with universality arguments. For the absolute values we find $\xi = (1.2 \pm 0.1) \times 10^{-8} \, \epsilon^{-0.65 \pm 0.02}$, $\epsilon_0 = [d/(5.7 \pm 0.6) \times 10^{-8}]^{-1.54 \pm 0.05}$, and $\xi \rho_s / T = (0.16 \pm 0.01) \times 10^{-8}$.

I. INTRODUCTION

Order-disorder transitions are of great theoretical and experimental interest in physics. The superfluid transition of liquid helium has been intensively investigated[1] in order to study critical phenomena at higher-order transitions. The reasons seem to be that liquid helium offers important advantages to the experimentalist: The liquid is extremely pure and homogeneous. In addition, it is possible to achieve a temperature stability, resolution and homogeneity of better than 1 μK. As a result, one can investigate a very sharp phase transition with a very high temperature resolution close to the transition temperature. The recent progress[2] in the theory of critical phenomena makes it worthwhile to perform an extensive test of theoretical predictions for the superfluid transition.

Liquid helium also offers the possibility for investigating the influence of pressure or impurities on the phase transition. Universality arguments[3] predict that these changes should not influence certain dimensionless parameters characterizing the transition because they do not influence the symmetry of the transition. The critical exponents, for example, should only depend upon such general properties of the system as its dimensionality and the degrees of freedom in the order parameter for the transition.[3] These concepts have been supported recently by explicit calculations.[2] Greywall and Ahlers have verified this prediction for the superfluid fraction ρ_s/ρ of ^{4}He under pressure.[4] This quantity is closely related to the order parameter for the superfluid transition.[5] On the other hand, Ahlers[6] has found an apparent violation of universality for the specific heat C_P of liquid helium near T_λ under pressure. According to his results, the amplitude ratio A/A' of the singularity of C_P above and below T_λ is pressure dependent, in contradiction to the universality concept. It seemed to be of importance to us to investigate more parameters for the superfluid transition under pressure.

In this paper we report measurements of the temperature $T_0(P)$ for the onset of superfluidity in $d = 0.1$-, 0.2-, 0.4-, and 0.6-μm-wide channels at pressures between saturated vapor pressure and the melting curve. We used porous membranes as second-sound transducers.[7] The onset of superfluidity in the channels of these membranes was detected by observing the presence or absence of second sound in a resonant cavity as a function of temperature at several fixed pressures. In order for vibrating filter papers to generate or detect second sound, the diameter of the channels must be smaller than the viscous penetration length of the normal fluid component and larger than the correlation length of He II, so that the normal fluid is pushed back and forth, while the superfluid can flow through the vibrating paper. When the temperature is raised the correlation length increases, and eventually near T_λ it becomes comparable to the channel diameter. Then, superfluidity is expected to vanish in the channel.[8,9] At that temperature the channels are "closed" for the superfluid component of He II as well. The filter paper is then not suitable for the production or

detection of second sound because it is no longer
a superleak. This effect has been pointed out by
Williams *et al.*[7]

We have measured the temperature at which the
second-sound signal in "filter-paper resonators"
vanished for different pressures and for papers
with different channel diameters. The disappear-
ance of second sound indicates how far the super-
fluid transition had been shifted below T_λ by the
restriction of the geometry. The results are valid
at least for the temperature range where the onset
of superfluidity occurred in our channels, 4×10^{-5} K
$\leqslant T_\lambda(P) - T \leqslant 4 \times 10^{-4}$ K. We find the reduced tran-
sition temperature depression $\epsilon_0 = 1 - T_0(P)/T_\lambda(P)$
to be independent of pressure to within our resolu-
tion of $\pm 2\%$. From our results for ϵ_0 we calculate
the exponent λ' and the coefficient d^* for ϵ_0
$= (d/d^*)^{-\lambda'}$. Through a scaling argument the onset
length of the channels is related to the correlation
length $\xi = \xi^* \epsilon^{-\nu'}$ of He II. We find that the co-
efficients ξ^* and d^* and the temperature exponents
λ' and ν' are not influenced, to within our resolu-
tion of $\pm 2\%$, by applying pressure to the liquid.
The pressure independence of λ' and ν' is in agree-
ment with universality. On the basis of a theoret-
ical prediction,[10, 11] it can be expected that $\xi \rho_s/T$
is a constant, independent of P and T. This pre-
diction has already been verified at vapor pres-
sure.[12, 13] We find $\xi \rho_s/T$ (as well as ρ_s/T) to be
independent of pressure to within $\pm 2\%$, as well.
All our results are, within their errors, in agree-
ment with theoretical predictions.

In Sec. II of this paper we present the details of
the experimental setup and technique. There we
discuss a technique for precise pressure regulation
at low temperatures. The performance of the
experiments, the data analysis and checks of the
data are discussed in Sec. III. Finally, in Sec. IV,
we discuss the results of our measurements and
compare them with measurements by others and
with theoretical predictions.

II. EXPERIMENT

A. Low-temperature setup

The complete experimental low-temperature
apparatus is shown in Fig. 1. It consists of a
copper pressure cell filled with liquid helium and
sealed by lead O rings. There are two second-
sound resonators (R_1 and R_2) and a sealed germa-
nium thermometer (T) inside this cell. All elec-
trical leads to the resonators and to the thermom-
eter passed out of the cell through Expoxy-filled
capillaries soldered into the cell body. Directly
connected to the pressure cell is a capacitive
transducer which measured the pressure of the
liquid in the cell. This whole assembly is sus-

pended inside a vacuum can which is surrounded
by the main helium bath. We kept about 7×10^{-3}
Torr of He gas in the "vacuum" can to provide
some thermal coupling between sample cell and
main bath. The temperature of the main bath was
usually kept 20–30 mK below $T_\lambda(P)$ and was
regulated to ± 0.1 μK. The helium sample (about
9 cm^3) in the cell and resonators is connected via
a capillary to a helium-filled pressure bomb of
about 8 cm^3 volume. This bomb is suspended
in its own vacuum can, which is also surrounded
by the main helium bath. It is used to produce and
regulate the pressure in the sample.

B. Pressure system

We want to describe the pressure regulating
system, whose main parts are shown in Fig. 1, in
some detail. A capacitive pressure transducer of
the Straty-Adams type[14] is attached directly to the
sample of pressurized helium being studied. The
helium sample is connected via a capillary to a
pressure bomb which is filled with liquid helium
and wrapped with a heater. This connection is via
room temperature, where a gauge is used to
measure the absolute pressure to ± 0.03 bar.[15] The
agreement (see Table II) between the measured
λ temperatures and those calculated from the
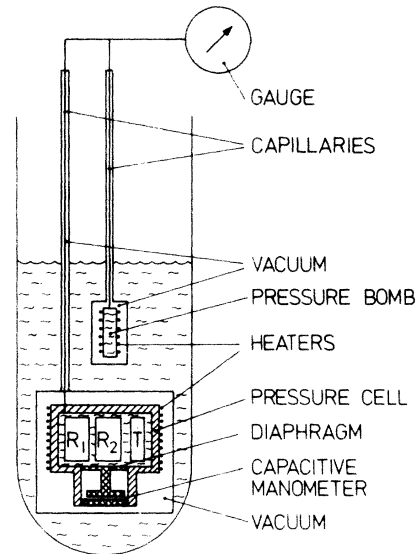measured pressures with the equation given by

FIG. 1. Experimental apparatus. R_1 and R_2 are the
two second-sound resonators and T is the germanium
thermometer. Capillary dimensions: Room tempera-
ture to bomb, 1-mm i.d.; room temperature to ex-
change-gas-can flange, 0.8-mm i.d.; flange to sample
cell, 0.2-mm i.d.

Kierstead,[16] showed the validity of the calibration of our gauge. The pressure cell, the pressure bomb, and the capillaries are each in vacuum-isolation cans or tubes which are immersed in the liquid-helium bath.

The bomb was kept in a temperature range where the thermal-expansion coefficient of helium is positive. Then passing a current through the heater increases the temperature of the bomb, thus raising the pressure in the entire liquid-gas system. The amount of heat necessary to keep the pressure in the sample constant is determined by the capacitive strain gauge. Its capacitance is measured using the bridge circuit shown in Fig. 2 with a lock-in amplifier as null detector. Any deviation in pressure at the sample produces an off-balance in the capacitance bridge and hence a nonzero voltage at the output of the lock-in amplifier. This voltage is power amplified and applied to the bomb heater in series with a dc bias current. This negative feedback loop automatically compensates for changes in the sample temperature, as well as less easily controlled conditions, such as the temperature profile in the helium Dewar. In addition, this method does away with the usual large room-temperature pressure tank whose temperature must be regulated extremely well to avoid straying from the isobar.

The strain gauge, made of Be-Cu heat-treated at 300 °C for 3 h, was built according to the Straty-Adams design.[14] The diaphragm is 1.34 mm thick and 24 mm in diameter. It is connected to the movable plate of the capacitor (23 mm diam). A spacing of 0.075 mm at zero pressure yielded a capacitance of about 50 pF, which increased to about 100 pF at 30 atm. The sensitivity increased from 0.9 to 3.6 pF/bar over this pressure range. The movable and fixed plates of the capacitor were insulated from ground. Hence in this situation the GR Model 1615 capacitance bridge[17] can be used in a 3-terminal mode excluding lead capacitance from the measurement, and on the 100-pF range over the entire λ-line region. The temperature of the capacitance bridge was regulated to 0.01 °C to minimize drifts due to the temperature dependence of its components (5 ppm/°C). Coaxial leads[18] were used all the way between bridge and capacitor. They were run through a tube together with the heater and thermometer wires into the sample vacuum can. The capillary dimensions, described in the caption of Fig. 1, were chosen so that the system's time constant was about 0.3 sec.

The operational procedure was to condense enough helium gas into the pressure bomb to yield a pressure slightly less than twice the pressure sought. After waiting for at least 2 h the bomb was connected to the sample through a room-temperature valve, resulting in a pressure slightly below the pressure desired. A dc bias voltage is then applied to the bomb heater, which brings the system to the proper pressure. Finally, the capacitance bridge is balanced. The output from the bridge's null detector is connected in series with the dc bias such that an increase of pressure at the sample produces a decrease in the voltage across the heater. If a power amplifier is used on the output of the null detector whose gain is adjusted so that full-scale off-balance on the high-
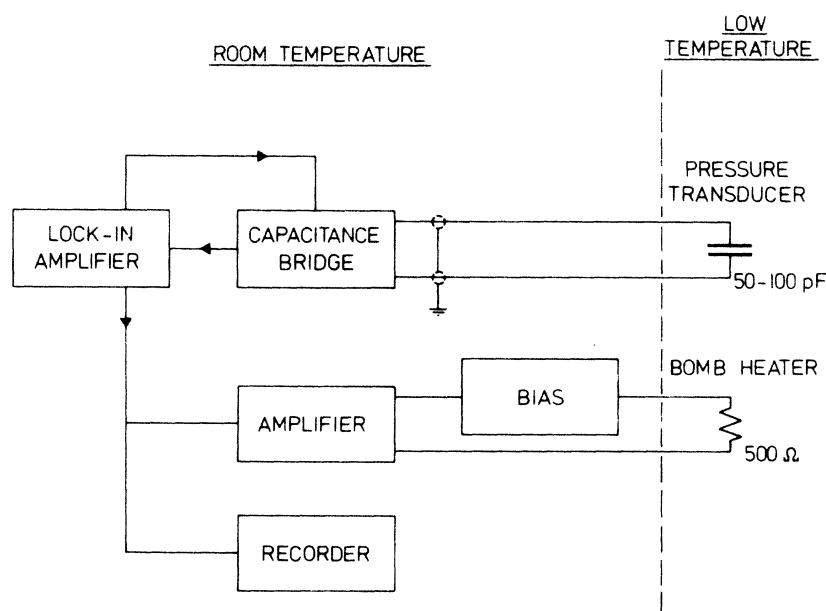

FIG. 2. Block diagram of the pressure regulating electronics.

pressure (high-capacitance) side reduces the voltage on the heater to zero, the system is essentially foolproof and can be left unattended as long as helium surrounds both the bomb and sample vacuum cans. The performance of the system is shown in Fig. 3. The present system provided short-term ($\tau = 1$ sec) pressure stability of 5×10^{-5} bar and long-term ($\tau = 2$ h) pressure stability of 10^{-5} bar. Taking the slope of the λ line, -55 atm/K $> (dP/dT)_\lambda > -120$ atm/K,[16] this corresponds to an uncertainty in the transition temperature of less than 0.2 μK.

The system can undoubtedly be improved if operation is desired over a smaller pressure range. This can be achieved by reducing the capacitor spacing in the pressure transducer so that at the highest pressure used the plates just fail to touch. Through the use of an external standard kept at helium temperatures, an appreciable reduction of drift can be expected. Since relative measurements are being made, any ratio-measuring device can be utilized in place of the GR bridge.[14] Finally, we drove the bridge at 0.2 V_{rms} at 5 kHz. The low drive was used to reduce cross talk encountered among various circuits in our particular experimental arrangement. Within reason, an increase in this drive voltage directly yields an increase in sensitivity of the pressure measurements. A capacitor system in which some of these improvements have been included showed a noise in $\Delta C/C$ of only 3×10^{-8} at a bridge voltage of 10 V.[19]

C. Thermometry and temperature regulation

A sealed germanium thermometer[20] was sitting in the liquid inside the pressure cell. Its value and

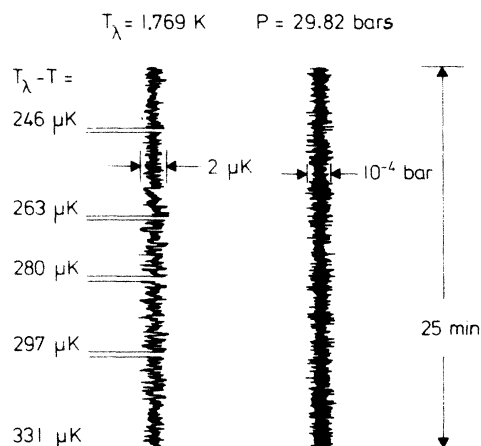

$T_\lambda = 1.769$ K $P = 29.82$ bars

FIG. 3. Strip-chart recording of the output of the lock-in amplifiers used with the sample thermometer (left) and the capacitive manometer (right) in the temperature- and pressure-regulating circuits of Figs. 2 and 4 during an actual data run at $P = 29.82$ bar. The spikes on the temperature recording are the transient response which occur when changing the ratio-transformer setting in order to change the sample temperature. These temperature changes do not influence the pressure regulation, as can be seen on the pressure recording.

sensitivity varied from 28.8 kΩ and 29.8 μK/Ω at the lower λ point to 51.7 kΩ and 11.7 μK/Ω at the upper λ point. The thermometer resistance was determined using the bridge circuit shown in Fig. 4, and operated at 29 Hz with a lock-in amplifier as null detector. The bridge ratio between the strongly-temperature-dependent resistance of the germanium thermometer and a very constant metal-film reference resistor ($R = 45$ kΩ) mounted
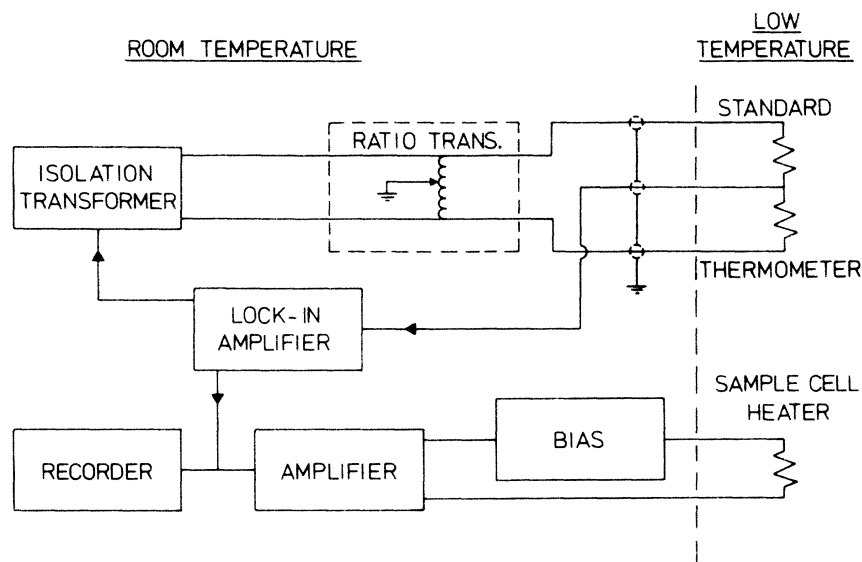

FIG. 4. Block diagram of the temperature regulating electronics.

on the sample cell was determined with a ratio transformer. A comparison of our λ-line determination with Kierstead's[16] results showed that the thermometer was unaffected by pressure (see Table II). The noise of this bridge circuit was about 10 nV$_{rms}$ (with 3-sec time constant). It was possible to resolve 0.3 μK with this setup. The off-balance output from the lock-in detector was amplified and applied to a heater wound around the pressure cell. This feedback loop kept the sample temperature constant to better than 0.3 μK, as can be seen in Fig. 3. The power dissipated in the thermometer was 1×10^{-9} W, and was checked to produce no measurable self-heating effects. The bridge ratio was calibrated against the 1958 ^{4}He vapor-pressure scale, using a capacitive manometer[21] for the vapor-pressure measurements.

The actual reduced-temperature difference $1 - T/T_\lambda(P)$ used in the analysis of the data was determined from the measured second-sound velocity u_2 by interpolating the original data of Greywall and Ahlers[4] for the velocity of second sound near T_λ under pressure. These values for $T_\lambda - T$ are good to 1 μK.[4] This technique was utilized in order that the second sound in the resonator provided both the sound amplitude and the temperature information. This freed us from depending on a thermometer mounted outside the resonators.

D. Sound electronics

A schematic of the electronic system for the sound measurements is shown in Fig. 5. The heart of the system is a wave analyzer[22]: a bandpass filter (3-Hz bandwidth), whose center frequency is tunable, followed by an rms voltmeter, which is used to detect the signal at the sound receiver. The analyzer also produces a sinusoidal output signal at the filter frequency for driving the sound generator. The frequency of the wave analyzer was mechanically swept at a constant speed of 3 Hz/sec to record the resonance spectrum of the second-sound resonators.

Both the sound generator and receiver have a bias voltage of about 100 V applied to them, so that the sound drive and detection are done at the same frequency. The electronic cross-talk between the drive and receiver circuits was reduced by careful shielding to about 100 nV$_{rms}$. However, since signals down to this level were being measured, it became important to understand how this cross-talk affected the sound amplitude. This understanding led to the installation of the phase shifter in the drive circuit, which is adjusted to maximize the amplitude of the particular resonant harmonic used for the data analysis. The details of this procedure are discussed in Sec. III B. The attenuator shown in Fig. 5 was used to check the dependence of the data on the drive amplitude (see Sec. III C).

The signal from the receiving transducer was amplified by 60 dB before being sent to the analyzer. The analog output from the analyzer, which is proportional to the amplitude of the signal, and the frequency from the counter after digital-to-analog conversion, were recorded separately as a function of time on a 2-pen strip-chart recorder

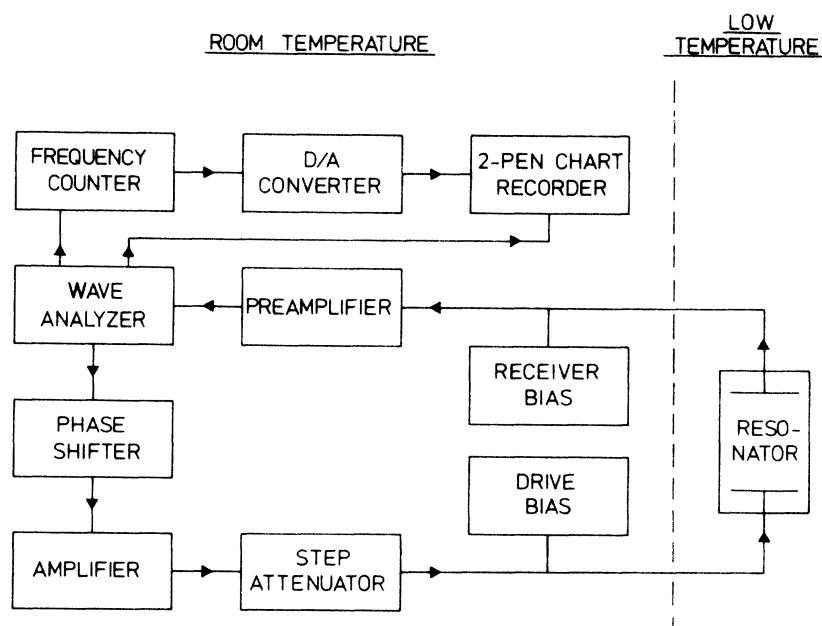ROOM TEMPERATURE   LOW TEMPERATURE

FIG. 5. Block diagram of sound electronics.

(see Fig. 5). As the frequency is swept linearly with time, the signal amplitude appears as a function of frequency as well. The frequencies and amplitudes of the resonances could be read from the recorder chart to within 1 Hz and 1% of full scale, respectively.

E. Second-sound resonators

With two similar electronic systems, sound was generated and detected simultaneously in two cylindrical cavities sitting inside the pressure cell (see Fig. 1). The design and dimensions of the stainless-steel resonators are given in Fig. 6. The height of the sample was kept to a minimum to avoid gravity effects.[23] The resonators were terminated at both ends by identical capacitive superleak transducers.[7] Their backing plates, serving as a stationary part of the condensers, were mounted with electrically insulating epoxy in the end caps. The surface of these plates was lapped with fine sand paper. The vibrating elements of the transducers were commercial "Nuclepore" filter papers.[24] They were plated with gold on one side to give a conducting layer with a thickness of about 300 Å and a resistivity of about 1 $\Omega/\square$. This conducting layer was electrically grounded to the resonator body. The helium sample entered the resonator by flowing between the end caps and resonator body. The two ends of each resonator body were ground flat and mutually parallel to 0.1%. The lengths of the resonators were measured at room temperature to $\pm 5 \times 10^{-3}$ mm and were corrected for thermal contraction due to cooling to helium temperatures. Both transducers in each resonator were biased with a dc voltage of about 100 V. The generator was driven at an ac voltage of 0.68 V$_{rms}$. The coaxial leads[18] for the drive signals and for the pickup signals were mounted in separate tubes. The velocity of second sound $u_2 = 2L\nu_n/n$ determined at SVP between 1.5 and 2.16 K from the resonant frequency ν_n of the nth harmonic, and the
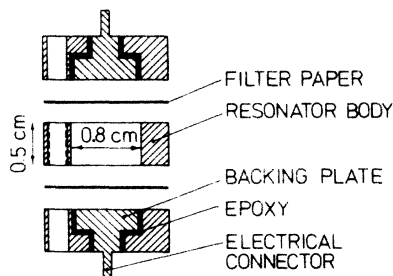

FILTER PAPER
RESONATOR BODY
0.8 cm
0.5 cm
BACKING PLATE
EPOXY
ELECTRICAL CONNECTOR

FIG. 6. Exploded cross-sectional view of sound resonator.

resonator length L agreed to $\pm 0.1\%$ with the data of Greywall and Ahlers.[4] Plane-wave modes dominated the spectra of our resonators. The so-called Bessel-function modes were absent in the frequency range over which our measurements were taken. The quality factor Q of the resonances defined as the resonant frequency ν divided by the full width $\Delta\nu$ at half-power was 1250 at 1.6 K. It decreased with increasing temperature to about 200 at $\epsilon = 70 \times 10^{-6}$, and remained constant to within the accuracy of our measurements in the temperature range $20 < 10^6 \times \epsilon < 70$.

F. Filter papers

The range for the channel diameter and channel density for three of the filter papers used in our experiment is given in Table I.[24] We have no corresponding information on GE 10 ($d = 0.1$ μm). Electron micrographs were taken on the filter papers used in our experiments. Unfortunately the scale calibration on the scanning-electron microscope used was not good enough to determine the channel diameter with an accuracy better than the range given in Table I for d. No estimate was possible for the 0.1-μm paper. Our pictures at least convinced us that the channels were circular and had very few interconnections. Transmission micrographs indicated that the channels are quite straight and of uniform diameter over the entire length. Because the diameters of the "holes" are a factor of 15–100 smaller than the thickness of the paper (10 μm), it is more reasonable to consider them as "channels" rather than as "pores" or "holes." We make the reasonable assumption that the channels are not changed by applying pressure to the surrounding liquid. Data taken at saturated vapor pressure (SVP) before and after the data at higher pressure had been obtained did agree within our resolution. In Table I we show how the efficiency of the transducers at temperatures clearly below $T_0(P)$ varied for different filter papers. We do not know whether the increase of the second-sound signal from the 0.6-μm paper to the 0.1-μm paper at constant drive voltage is due to the decrease of channel diameter or due to the increase of the number of channels (at constant total open area), or due to both. We discuss later how the efficiency of the resonators influenced our results.

III. DATA ACQUISITION AND ANALYSIS

A. Experimental procedure

After the system was prepared as described in Sec. IIB, the performance of the temperature- and pressure-regulating systems was checked and

TABLE I. Data on filter paper (Ref. 24).

Filter paper	Channel diameter (μm)	Channel density (10^7/cm^2)	Sound signal[a] (mV)
GE10	no information	no information	8
GE20	0.16-0.20	25.5-34.5	2.2
GE40	0.32-0.40	8.5-11.5	0.6
GE60	0.48-0.60	2.55-3.45	0.3

[a] Signal received at temperatures clearly below $T_0(P)$ and with a drive voltage of 0.68 V$_{rms}$.

their sensitivities measured. Then the pressure and temperature were regulated for about 2 h to ensure that equilibrium was achieved in the entire system. At about 1 mK below T_λ, the acoustic systems were checked by recording the resonant spectra of both resonators over a frequency range from about 100 Hz to 10 kHz. It was found that the operation of the resonators, transducers, and the over-all appearance of the resonant spectra were essentially pressure independent. In fact, the relative strengths of the various modes and their harmonics for a given resonator remained quite constant regardless of the pressure applied. Before any second-sound measurements were begun, the resistance of our thermometer at the λ transition was measured. This was done by observing the inflection point in the velocity of first sound as the apparatus was allowed to warm slowly (3 μK/min) through the λ point from below along an isobar.[25,26] We locked in on the fundamental plane-wave mode in order to measure the velocity of first sound. It was found that high-quality first sound could be generated in these resonators when the temperature was higher than that at which second sound vanished. A similar determination of the λ transition was made after all other measurements were finished. These λ-point measurements depend on the germanium-thermometer reproducibility, reference-resistor stability, and the pressure stability. The pressure stability in turn depends on the capacitive-pressure-transducer stability, reference-capacitor stability, and the operation of the pressure-regulating feedback system. Therefore the λ-point determination served as an over-all indication of the system's operation over long time periods, and was used to detect malfunctions in various components of the system, and in general to qualify the data taken during a given time period. Typically, the λ points measured at the beginning and end of a data run (about 10 h apart) agreed to within a few μK.

The data were acquired by holding the temperature constant, and sweeping the frequency of the second sound in a given resonator at a speed of 3 Hz/sec through at least five harmonics and re-

cording this part of the spectrum. For each filter-paper channel diameter d, a particular harmonic n was always included in this set on all isobars (n = 26 for d = 0.1 μm, n = 15 for d = 0.2 μm, n = 17 for 0.4 μm, and n = 35 for d = 0.6 μm). The amplitude and frequency of this harmonic were then measured as a function of temperature along an isobar. If the small-channel resonator was being studied, the frequency of the second sound in the large-channel resonator was simultaneously but independently swept and recorded, usually in the region of the tenth harmonic. This served as an additional check on the temperature, and aided in keeping track of harmonic numbers as the signal vanished in the small-channel resonator. If the large-channel resonator's second sound was under study, the other sound system was used to lock in on the fundamental first-sound resonance in the small-channel resonator, since second sound had already vanished in it. Then the velocity of the first sound was used for checking temperature

u_2 [cm/sec] =116.5   113.7   109.7   104.5   101.0

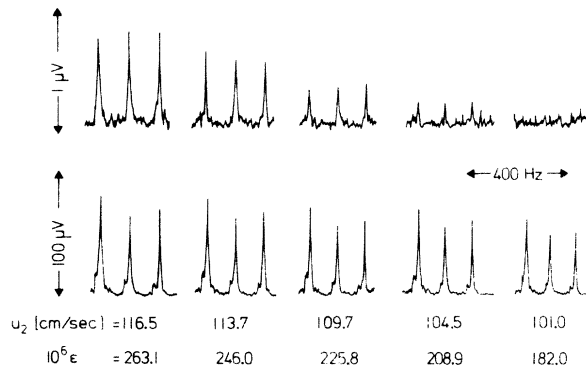$10^6\epsilon$ = 263.1   246.0   225.8   208.9   182.0

FIG. 7. Strip-chart (time) records of second-sound spectra. The sound amplitude is shown as a function of frequency, since the frequency is swept linearly in time (the frequency record has been suppressed). The top spectra show harmonics n = 25–27 from a resonator fitted with 0.1-μm paper. The bottom spectra are harmonics 10–13 from a resonator with 0.6-μm paper. The data were taken simultaneously with the two resonators along the isobar P = 29.82 bar. The temperature has been increased in four steps going from left to right and is given as $\epsilon = 1 - T/T_\lambda(P)$. The absolute frequencies involved can be obtained by calculating $\nu = u_2 n$.

stability. Recordings of second-sound amplitude versus frequency were started at a temperature below T_λ such that the sound amplitude was about 30 μV. Then the temperature was raised in steps of 50-2 μK, with spectra being recorded after thermal equilibrium had been reached at each step (a wait of about 2 min). An example of the results from this procedure is shown in Fig. 7. The upper traces in this figure show the amplitude of second sound in the 0.1-μm-channel-diam resonator as the temperature is increased until no second sound is discernible. The second-sound spectra in the lower traces in Fig. 7 were taken at the same time and under identical circumstances as the corresponding traces directly above it, except using a resonator fitted with 0.6-μm-channel-diam paper. The absolute amplitudes of the signals in the lower traces and their weak dependence on temperature in this region demonstrate that the channel diameter of the filter paper is controlling the amplitude of the second sound in the other resonator. At constant pressure the temperature was stepped up to the vanishing of the sound signals and back down to about 30-μV amplitudes at least twice. The amplitude of a particular harmonic was then plotted against the velocity of second sound obtained from measuring its frequency. Various plots of this nature are shown in Figs. 8-11.

The relative error in the amplitude measurements increases as the sound amplitude decreases, resulting in possible errors of about 100% at the lowest amplitudes measured (100 nV). However, regardless of the noise, even if a harmonic was barely discernible, its frequency was still resolvable to better than 1%. All error in the sound-cutoff determination is due to the uncertainty in the amplitude measurements because the uncer-

tainty in the velocity measurement was negligible.

It was found that the data close to the sound cutoff could be well described by the following equation:

$$\ln(A/A^*) = m(P)u_2 . \tag{1}$$

Here A is the sound amplitude, u_2 is the sound velocity, A^* is a constant for each filter paper independent of pressure, and $m(P)$ depends on pressure and filter-paper channel diameter. The logarithm of the amplitude versus velocity for second sound is plotted for the four channel diameters used at essentially constant pressure (0.06-0.2 bar) in Fig. 8. Here the range of validity of Eq. (1) can be seen to vary from amplitudes of 1 μV and less for the 0.6-μm channel paper data to 30 μV and less for the 0.1-μm data. If we extended the graph to higher velocities, it could be seen that the curves saturate for all filter papers similar to that shown here for the 0.6-μm paper. The amplitudes at which this saturation occurs increase for decreasing channel sizes, so that far away from T_λ the 0.1-μm filter paper will produce second sound more than an order of magnitude stronger than the 0.6-μm paper (all other variables equal). The values for the amplitudes at saturation are given in Table I. An increase of the slope $m(P)$ with increasing channel diameter is also clearly present and will be discussed in Sec. III C. Figure 9 gives the same type of plot but for constant channel diameter (0.6 μm) with pressure as the variable parameter. Although all the curves have the same shape, it can be seen that m increased with increasing pressure. This will be discussed further in Sec. III C. The sound amplitude at constant drive voltage also increased with increasing pressure for the 0.6-μm filter paper (see Fig. 9). The viscous penetration length λ_n of
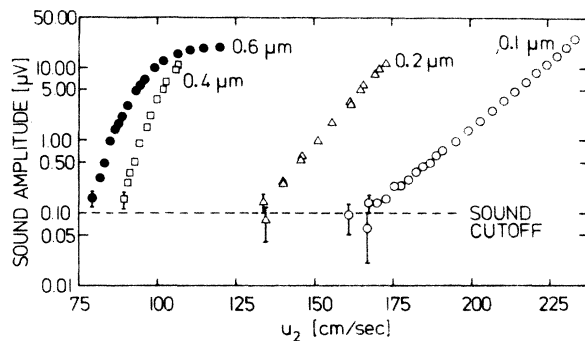

FIG. 8. Second-sound amplitude as a function of second-sound velocity u_2, for the four filter papers used. The points are labeled by the channel diameter of the filter papers. The pressure is constant within the accuracy of the diagram (0.05-0.2 bar). The cutoff level used for determining $u_{2,0}$ is indicated.
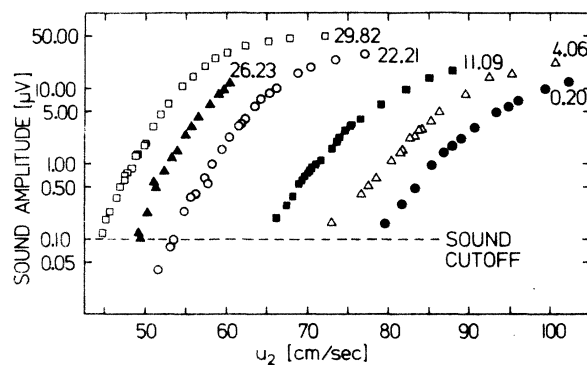

FIG. 9. Second-sound amplitude as a function of second-sound velocity u_2. The data were taken with 0.6-μm filter paper under the pressure (in bar) associated with each set of data points. The sound cutoff level used for determining $u_{2,0}$ is indicated.

the normal component is about 1 μm at SVP and the frequencies used (3.5 kHz) for the run with this paper. Because for this paper λ_n is comparable to the channel diameter, there might occur some slippage of the normal component in the channels resulting in a decrease of sound amplitude. The increase of viscosity with increasing pressure will reduce the slippage and could be responsible for the increase of sound amplitude with pressure. This effect should not influence the sound amplitude in resonators equipped with paper with smaller channels. We will come back to the pressure dependence of the sound amplitude when we discuss the data in Sec. IV A.

B. Phase adjustment

When using a sound drive of the order of volts and detecting sound of the order of hundreds of nanovolts at the same frequency, the system has to be shielded well to avoid coupling between the drive and receiver circuits. In our apparatus we encountered cross-talk of about 100 nV whose magnitude and phase were weakly dependent on frequency, and which can be described at a given frequency in polar coordinates by the vector (B, φ_B).

As the frequency of the sound is swept through a particular harmonic in a resonator, the signal increases from zero to some peak amplitude A and then decreases to zero, while the phase of the resulting sound signal changes through 180°. Such a signal can be described in polar coordinates by the vector $(A \sin\varphi_A, \varphi_A)$, where $\varphi_A = 90°$ or 270° at the peak, depending on whether the harmonic is odd or even. The wave analyzer measures the sum of this and the background signal:

$$S = [A^2 \sin^2\varphi_A + 2AB \sin\varphi_A \cos(\varphi_A - \varphi_B) + B^2]^{1/2}.$$

$$(2)$$

Since A is the actual sound amplitude being measured, B, φ_B, and φ_A must be known to extract A from S. However, if one would set $\varphi_B = 90°$, and measure the amplitude at the peak where $\varphi_A = 90°$ or 270°, one obtains the simplified version $S = A \pm B$ or $A = S \pm B$, for Eq. (2); the plus-or-minus signs applying to alternate harmonics. Then by measuring the peak amplitude S at a frequency ν and then the background level B at the same frequency ν after the second sound has vanished, A can be obtained. Notice that if the phase in the sound circuit is peaked for a particular harmonic n,

$$A_n = S_n - B,$$

$$(3)$$

while its two closest neighboring harmonics $n + 1$ and $n - 1$ will be minimized, yielding

$$A_{n \pm 1} = S_{n \pm 1} + B.$$

$$(4)$$

Equation (3) shows that with this phase setting the sound signal for the nth harmonic *adds* to the background, making amplitude measurements possible to a level limited only by the electronic noise. For the $n+1$ and $n-1$ harmonic [Eq. (4)], the resonant peak will actually be a dip when $A < 2B$, and the spectrum will dip to the zero voltage level when $A = B$ with this phase setting. [For $A < B$, Eq. (3) is not directly applicable]. For random-phase adjustments almost any type of spectrum can be observed.

In a few early runs the phase was not adjusted properly, but the background phase and amplitude were carefully measured as a function of frequency. In general these quantities could be described by first-order polynomials in the frequency:

$$B = b_0 + b_1\nu, \quad \varphi_B = c_0 + c_1\nu.$$

Then these equations and Eq. (2) were used with the total amplitude S and frequency ν measured to obtain A for each data point. Later the following technique was used: As mentioned above, the phase and amplitude of the background signal B were weakly frequency-dependent. Therefore, before any measurements were made the temperature was stabilized near, but slightly below, where the sound vanished, and the phase shifter adjusted to maximize the amplitude of the harmonic under study. Thus, with this procedure, the phase adjustment is correct for the smallest amplitudes when its effect is most important. That is, as one cools away from the cutoff temperature, the sound amplitude increases relative to the background level (which actually falls very slightly with increasing frequency or temperature), making the background progressively less important. The results of this method were checked against those obtained using the first method by using two different phase settings in one run. The agreement was well within the precision of the measurements.

C. Checks

1. Harmonic dependence

As stated in part A of this section, for each channel diameter a particular harmonic number was used for all measurements. We tested whether our results could depend on the harmonic chosen by measuring sound amplitudes and velocities in each resonator for several harmonic numbers and at various pressures. It was found that although a resonator usually yields a spectrum with harmonics of varying amplitudes at temperatures far away from T_λ, as a temperature close to

where the sound vanishes is reached, all harmonics assume nearly the same amplitude. A plot of sound amplitude versus velocity of four harmonics from $n = 20$ to 35 in the 0.6-μm-pore-size resonator is presented in Fig. 10. Fitting Eq. (1) over the applicable range of each data set yields velocity cutoffs which vary less than 1%, even though the frequency at which the data were taken differs by more than 1000 Hz. This indeed demonstrates that within the experimental errors, the cutoff velocity does not depend on harmonic number. Regardless, as mentioned earlier, all measurements with a given filter paper were made with the same harmonic.

2. Sound drive amplitude

The effect of varying the voltage applied to the sound-drive transducer was investigated over the range from 0.0745 to 6.3 V_{rms}. First, it was found that the second-sound velocity was independent of the drive voltage with all other variables held constant. However, at the highest drive used (6.3 V_{rms}), slight heating of the resonators was observed (~0.5 μK). A test was then done for critical velocity effects with drives between 0.0745 and 2.08 V_{rms} where no heating was detectable.

The intrinsic critical velocity of superfluid helium decreases strongly near the λ transition or near the temperature where superfluidity vanishes in a particular geometry.[27] An order-of-magnitude estimate gave a maximum velocity of 10^{-2} cm/sec for the motion of the filter paper at 1 V ac drive and 100 V bias (at constant frequency this velocity is proportional to the product of the drive and bias voltages). Therefore, at all temperatures of the experiment the velocity of the filter paper should have been small compared to the critical velocity
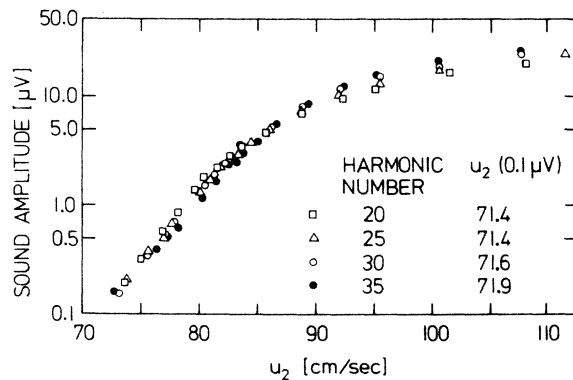
of He II, ($v_{int} = 380$ $\epsilon^{0.68\pm0.03}$ at SVP according to Ref. 27).

However, if critical velocities were being reached in the filter-paper channels of the transducers, the sound signal should have decreased with increasing drive voltage, owing to the reduced efficiency of the sound transducers. This would lead to a higher cutoff velocity being measured, since the sound signal at a given temperature would be reduced. In fact, as can be seen in Fig. 11, the opposite was observed; each time the drive voltage was increased by a factor of 3, we observe the same relative decrease in cutoff velocity of about 3.3%. The figure demonstrates that the cutoff velocity is a rather weak function of the drive voltage. However, the sound drive was fixed at 0.68 V_{rms} for all the data in Table I and in the figures from which our conclusions were obtained. The drive and receiver bias voltages were also constant throughout the measurement. Similar tests were done with the various filter papers and at various pressures. We could exclude any nonlinear or critical velocity effects as influencing our results.

3. Cutoff level

The frequency at which the amplitude of second sound intercepted the 0.1-μV noise level was taken as the cutoff where the sound "vanished" for our apparatus. The 0.1-μV level is a somewhat arbitrary cutoff, and the absolute cutoff velocity and temperature involved would be slightly different for different noise levels. The dependence of our results on this cutoff level has been investigated.
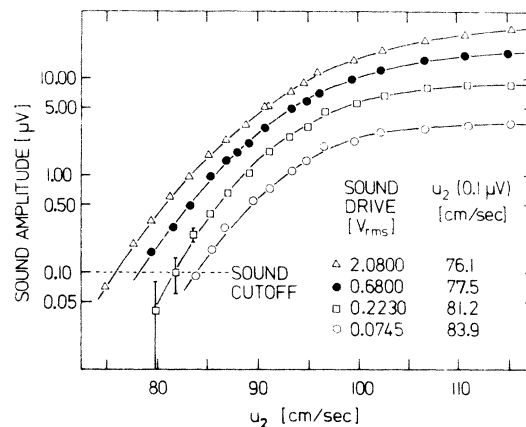

FIG. 10. Second-sound amplitude for four harmonics as a function of second-sound velocity at $P = 4.063$ bar using 0.6-μm filter paper. The inset shows that the cutoff velocity $u_2(0.1 \mu V)$ is essentially independent of the second-sound harmonic used.

FIG. 11. Second-sound amplitude for various drive voltages as a function of velocity of second sound at $P = 0.2$ bar using 0.6-μm filter paper. The sound cutoff used for determining $u_{2,0}$ is indicated. The inset shows the weak dependence of $u_{2,0} = u_2(0.1 \mu V)$ on the sound drive voltage.

The basic question is: What happens to the velocity $u_{2,0}$ of sound measured at the amplitude cutoff level, for various cutoff levels?

As stated in Sec. III A, the data for the second-sound amplitude as a function of frequency close to the sound cutoff can be described by Eq. (1). Also, within the precision of our data, the velocity of second sound can be described by a simple power law, [4,28]

$$u_2 = h(P)\epsilon^{\Phi}, \tag{5}$$

where $\epsilon = 1 - T/T_\lambda$, Φ is pressure independent for the accuracy of our experiment, and

$$h(P) = h_1 + h_2 P. \tag{6}$$

Substituting Eq. (5) into Eq. (1) we have

$$\ln(A/A^*) = m(P)h(P)\epsilon^{\Phi}. \tag{7}$$

Experimentally we find A^* to be a function of filter-paper channel diameter only (independent of pressure). Therefore, if

$$m^{-1}(P) = \alpha h(P), \tag{8}$$

where α is a constant of proportionality, then constant A (sound amplitude) in Eq. (7) always implies constant ϵ independent of pressure. Figure 12 shows $m^{-1}(P)$ taken from our data (see for example Figs. 8 and 9), where Eq. (1) is valid as a function

of pressure. The linear curves on this graph show $\alpha u_{2,0}$, a quantity proportional to the velocity of second sound at constant ϵ, which is therefore proportional to $h(P)$ in Eq. (5). The proportionality factor has been chosen for each channel diameter so that the curves and data points coincide for ease of comparison. It can be seen that the condition in Eq. (8) is satisfied. Therefore, regardless of which cutoff level is used for the analysis [limited only to the part of the data for which Eq. (1) is valid], our result that $m^{-1}(P) \propto u_{2,0}(P)$ indicates that a given filter-paper channel diameter will yield a constant ϵ at cutoff, independent of pressure. As will be seen in Sec. IV, the validity of Eq. (1) and Eq. (8) is a sufficient condition for most of our conclusions, in particular those regarding the pressure dependence of the various quantities investigated.

IV. RESULTS AND DISCUSSION

As will be shown in the following, the onset of superfluidity in the channels used occurred in the temperature range of 4×10^{-5} K $\leqslant T_\lambda(P) - T \leqslant 4 \times10^{-4}$ K or $2\times10^{-5} \leqslant \epsilon \leqslant 2\times10^{-4}$. Hence all the results to be presented below are valid for at least this temperature range and for pressures between saturated vapor pressure and the melting curve of ^{4}He.

A. Pressure dependence

The measurements and the data analysis described in the above sections yield, for each of the four filter papers used, a set of frequencies
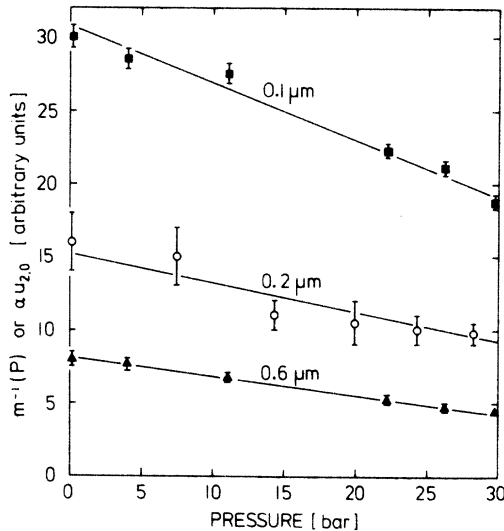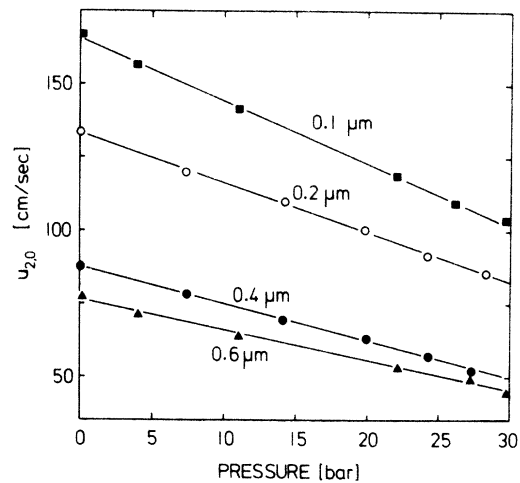

FIG. 12. Reciprocal of the slope m^{-1} (points) of Eq. (1) and $\alpha u_{2,0}$ (lines) as a function of pressure. The points for m^{-1} are labeled by the filter-paper channel diameter. The 0.4-μm channel-size data have been suppressed for clarity. $\alpha u_{2,0}$ is proportional to the velocity of second sound at constant ϵ and is therefore proportional to $h(P)$ in Eq. (5). The factor α is adjusted so that the resulting curve for $\alpha u_{2,0}$ falls near the data for m^{-1} for ease of comparison.

FIG. 13. Velocity of second sound at an amplitude of 0.1 μV (sound cutoff level) as a function of pressure. Each data set is labeled by the channel diameter of the filter paper used. The straight lines are an aid for the eyes.

TABLE II. Experimental results.

P (bar)	$T_{\lambda,K}$ [a] (K)	T_λ [b] (K)	$u_{2,0}(\pm\Delta u_{2,0})$ (cm/sec)	$10^6\epsilon_0(\pm10^6\Delta\epsilon_0)$	$10^3\rho_{s,0}/\rho$	$10^4\rho_{s,0}/T$ (g/cm^{3}K)	$10^8 d\rho_{s,0}/T$ (g/cm^{2}K)
			$d=0.1\,\mu$m				
0.203	2.171	2.171	166.8(1.3)	187.0(4.4)	7.80	5.26	0.526
4.063	2.132	2.132	155.9(1.0)	183.6(3.5)	7.29	5.25	0.525
11.086	2.050	2.049	140.5(1.1)	186.8(4.4)	6.66	5.29	0.529
22.212	1.894	1.893	117.3(2.1)	184.6(9.9)	5.70	5.23	0.523
26.234	1.830	1.829	108.3(1.1)	181.5(5.5)	5.36	5.19	0.519
29.821	1.769	1.767	102.3(1.2)	186.5(6.5)	5.27	5.37	0.537
mean value	···	···	···	185.0	···	5.25	0.525
			$d=0.2\,\mu$m				
0.101	2.172		133.6(0.8)	103.4(1.9)	5.26	3.55	0.709
7.448	2.094		119.4(1.0)	103.0(2.6)	4.78	3.61	0.722
14.288	2.008		109.5(1.1)	109.0(3.3)	4.47	3.71	0.741
19.901	1.929		100.0(1.1)	110.0(3.6)	4.13	3.68	0.736
24.238	1.863		91.4(1.2)	106.8(4.2)	3.80	3.58	0.717
28.291	1.796		85.3(1.0)	110.0(3.9)	3.67	3.66	0.732
mean value	···		···	107.0	···	3.63	0.726
			$d=0.4\,\mu$m				
0.051	2.172		87.7(0.4)	34.2(0.5)	2.47	1.66	0.665
0.051	2.172		87.6(1.2)	34.0(1.4)	2.46	1.66	0.663
7.448	2.094		78.1(1.1)	33.4(1.4)	2.24	1.69	0.677
14.146	2.010		69.1(1.1)	31.9(1.5)	1.97	1.63	0.650
19.901	1.929		63.1(1.0)	32.5(1.5)	1.82	1.62	0.649
24.238	1.863		57.0(1.0)	30.4(1.6)	1.64	1.55	0.618
28.271	1.796		52.1(1.6)	29.5(2.7)	1.53	1.52	0.609
mean value	···		···	32.3	···	1.62	0.647
			$d=0.6\,\mu$m				
0.203	2.171	2.171	77.5(0.8)	24.7(0.8)	1.98	1.34	0.802
4.063	2.132	2.132	71.6(0.4)	23.4(0.4)	1.82	1.31	0.785
11.086	2.050	2.049	64.1(0.4)	23.1(0.4)	1.65	1.31	0.784
22.212	1.894	1.893	53.2(0.4)	22.9(0.5)	1.40	1.28	0.770
26.234	1.830	1.829	49.0(0.5)	22.6(0.7)	1.31	1.27	0.760
29.821	1.769	1.767	44.5(0.8)	21.1(1.1)	1.20	1.22	0.731
mean value	···	···	···	23.0	···	1.29	0.772

[a] $T_{\lambda,K}$ was calculated from the measured pressures P with the equation given in Ref. 16.
[b] T_λ was measured in this experiment.

ν_0 of second sound at various pressures from SVP to the melting curve at which second sound vanished. The frequencies ν_0 were multiplied by twice the length L of the resonators to give the second-sound velocity $u_{2,0}$ at onset of superfluidity in the channels. These data are given in column 4 of Table II. The errors given there arise from the uncertainty in determining the second-sound amplitude when the signals fall into the cutoff noise level of 0.1 μV and the uncertainty for the length of the resonators $(\Delta L/L = 10^{-3})$. The

smallest measured velocities were about 45 cm/sec. In Fig. 13 we show the velocity $u_{2,0}$ of second sound at cutoff as a function of pressure for the four filter papers. Within the errors, $u_{2,0}$ is a linear function of pressure (as is obvious from Fig. 12 already). The data of Greywall and Ahlers[4] show that $u_{2,0}$ is a linear function of P at constant ϵ (to about 2% or better for $P < 30$ bar and $2\times10^{-5} < \epsilon < 2\times10^{-4}$).[28] Therefore the data for $u_{2,0}$ presented in Table II and Fig. 13 suggest that ϵ at onset is independent of pressure, as was already ex-

pected from the argument presented in Sec. III C 3. This was verified explicitly by calculating $\epsilon_0 = 1 - T_0(P)/T_\lambda(P)$ from the measured velocities of second sound at onset. These values for ϵ_0 were determined from the original data for $u_2(\epsilon)$ of Ref. 4 and our measured $u_{2,0}$. They are given in Table II. The errors for ϵ_0 given in the table are calculated according to $\Delta\epsilon_0/\epsilon_0 = 3\Delta u_{2,0}/u_{2,0}$; the additional error arising from an uncertainty of 1 μK for T_λ in the data of Ref. 4 has not been included into the errors given for our data for ϵ_0. The results for $\epsilon_0 = 1 - T_0(P)/T_\lambda(P)$ are plotted as a function of pressure in Fig. 14. The somewhat larger spread in the results from the run with the 0.4-μm paper compared to the other runs may be attributed to the fact that these were the first data taken. In the later experiments with the other three filter papers, the experience gathered during the first runs and slightly improved equipment resulted in improved data. There seems to be a slight trend with pressure toward larger ϵ_0 in the data taken with the 0.2-μm paper and toward smaller ϵ_0 in the data taken with the 0.4- and 0.6-μm papers. We cannot establish a pressure dependence of ϵ_0 outside of our errors, and suggest a possible reason for the trend of the data taken with the 0.4- and 0.6-μm papers. As can be seen in Fig. 9, for example, the sound amplitude at constant-drive voltage increased by a factor of 2.5 between SVP and the melting curve for the 0.6-μm paper. An argument for this increase was discussed in Sec. III A. The increase of sound amplitude with pressure will result in a decrease of ϵ_0, as observed for the 0.4- and for the 0.6-μm
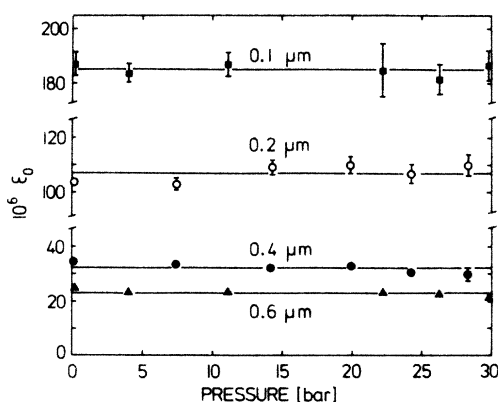

FIG. 14. Reduced transition temperature depression $\epsilon_0 = 1 - T_0(P)/T_\lambda(P)$ at the vanishing of the second-sound signal as a function of pressure. Each set of data is labeled by the channel diameter of the filter paper used. Horizontal lines are drawn through the average value of ϵ_0 for each set. Error bars are shown only when they are larger than the data point. Note the discontinuous vertical scale.

papers. From the discussion given in Sec. III C 2 we conclude that the change for ϵ_0 resulting from an increase of sound amplitude by a factor of 2.5 over the full pressure range should be as much as (7–10)%.

From all the data shown in Fig. 14 we conclude that for a given channel diameter d the reduced onset temperature depression ϵ_0 is independent of pressure within the errors from saturated vapor pressure to the melting curve:

$$\epsilon_0(P) = \text{const} \pm 2\%. \tag{9}$$

This is the main result of our experiments on which the further conclusions about pressure dependences rely.

Greywall and Ahlers[4] invoked higher-order correction terms in ϵ in addition to the leading term in the power-law expansions for u_2 and ρ_s/ρ to explain their data. If they present their data as $\rho_s/\rho \propto \epsilon^\zeta$, then the apparent exponent ζ varies between about 0.668 and 0.683. This was also observed by Terui and Ikushima.[29] The trend for the data of Ref. 4 is not quite monotonic with pressure. The variation of the apparent exponent ζ is smaller than our error for ϵ_0 and for the quantities to be discussed below. We can therefore not decide from our data if the inclusion of higher-order correction terms is necessary to describe our data. In addition, the small temperature range $2 \times 10^{-5} \lesssim \epsilon \lesssim 2 \times 10^{-4}$ for our experiment may make such a decision difficult even for more accurate results. The higher-order correction term for u_2 is only of the order of a few percent for the ϵ range of our experiment.[4,28] For the analysis of our results and for the calculation of the uncertainties we assume pure power-law representation of the quantities near T_λ.

It is easy to show then that the coefficient d^* as well as the exponent λ' in the relation[8,9]

$$\epsilon_0 = (d/d^*)^{-\lambda'} \tag{10}$$

(d^* is the channel diameter for an onset temperature $T_0 = 0$) have to be independent of pressure. We have ϵ_0 and d as independent of pressure. Comparing the results taken with two filter papers with channel diameters d_1 and d_2, we can write with Eq. (10)

$$\lambda' = -\log(\epsilon_{0,1}/\epsilon_{0,2})/\log(d_1/d_2).$$

Here $\epsilon_{0,i}$ is the reduced temperature shift in a channel with diameter d_i. The data in Fig. 14 show that $\epsilon_{0,1}/\epsilon_{0,2} = \text{const}$ independent of pressure. Therefore the exponent λ' has to be independent of pressure. Taking the uncertainty of $\pm 2\%$ for the pressure independence of ϵ_0 into account, we find from the above equations that for

all pressures

$$\lambda'(P) = \text{const} \pm 2\%. \tag{11}$$

The result that the critical exponent λ' is independent of pressure is in agreement with the principle of universality for continuous phase transitions as, for example, proposed by Kadanoff.[3] This principle predicts that changing an inert variable, like the pressure for the superfluid transition, will not affect the symmetry of the system and thus leaves the critical exponents unchanged. The more explicit statement[2] is that critical exponents are expected to depend only upon such general properties as the spatial dimensionality of the system and the degrees of freedom of the order parameter. In superfluid helium, both are not influenced by pressure, so that λ' is expected to be independent of pressure in agreement with our experimental results. Because ϵ_0, d, and λ' are independent of pressure, we must have also

$$d^*(P) = \text{const} \pm 2\%. \tag{12}$$

The error for d^* is obtained by fixing $\lambda'(P)$ without any uncertainty, and considering only the uncertainty in Eq. (9).

According to scaling[30] there should be only one intrinsic length describing the characteristic properties near the phase transition. This should be the bulk-correlation length. Other lengths, such as the length describing surface properties, or the onset length in finite geometries, should only differ from this length by factors of order unity, but are expected to have the same temperature exponent.[1,8,9,31] The correlation length can be written as a power law in the distance $\epsilon = (T_\lambda - T)/T_\lambda$ from the transition temperature,

$$\xi = \xi^* \epsilon^{-\nu'}. \tag{13}$$

We know of no theory possibly applicable to He II which relates a depression of the transition temperature to the correlation length, or which gives the factor between the onset length and the correlation length, besides the phenomenological Ginzburg-Pitaevskii-Mamaladze theory.[8] We are aware of the reservations for applying this phenomenological theory to He II.[31] To relate our results for the depression of the transition temperature to the correlation length of superfluid helium, we use the prediction that the transition at T_0 occurs when a characteristic length ξ for the superfluid state becomes comparable to the channel diameter d, with $\xi(T_0) = \gamma d$. We use the numerical value given in Ref. 8 for the constant γ. There it is predicted that superfluidity vanishes in a cylindrical channel of diameter d when

$$\xi_0 = \xi(T_0) = 0.207d, \tag{14}$$

which implies that $\nu' = 1/\lambda'$. If this equation is fulfilled the channels in our filter paper are "closed" to the superfluid as well as to the normal fluid. We have shown above that ϵ_0, λ', and d^* are, within their errors, not influenced by applying pressure to He II. Therefore also ν' and ξ^*, and hence the correlation length ξ itself, are independent of pressure. Lines of constant ϵ are also lines of constant ξ. The pressure independence of not only the exponent ν' but the correlation length itself goes beyond predictions of scaling[2,30] and universality.[3]

From the definition of the correlation length ξ by Ferrell et al.[10] and by Halperin and Hohenberg[11] it follows that

$$\xi \rho_s / T = m_4^2 \, k_B / 4\pi\hbar^2 = 0.044 \text{ g/cm}^2\text{K}, \tag{15}$$

where all symbols have their usual meaning. We have investigated the pressure independence of this quantity. Since for all our results $T_\lambda(P) > T > T_\lambda(P) - 4\times 10^{-4}$ K we can set $T \simeq T_\lambda(P)$ in Eq. (15). We have shown above that ξ is independent of pressure. At the onset temperatures for superfluidity in the channels, we have $\xi_0 = \gamma d = \text{const}$ at all pressures. Therefore the quantity (ρ_s/T) at onset has to be independent of pressure if the above Eq. (15) is valid for all pressures. For this test we have calculated $(\rho_{s,0}/\rho)$ from our measured $u_{2,0}$, using thermodynamic data for C_P and the entropy S,[1,6] and the relation between ρ_s and u_2 given by linear two-fluid hydrodynamics.[32] The resulting values are shown in column 6 of Table II. The errors for $\rho_{s,0}$ are $\Delta\rho_{s,0}/\rho_{s,0} = 2\Delta u_{2,0}/u_{2,0} + (4\%$ from the uncertainties in C_P and S). Using these values for $(\rho_{s,0}/\rho)$ and the data of Kierstead[16] for $T_\lambda(P)$ and $\rho(P)$ we have calculated $\rho_{s,0}/T$ as well as $d\rho_{s,0}/T$ [with $T = T_\lambda(P)$]. These data are given in the last two columns of Table II. The values for $d\rho_{s,0}/T$ are plotted as a function of pressure in Fig. 15. The figure shows that $d\rho_{s,0}/T$ is independent of pressure. The fact that the data for different filter papers do not coincide is attributed to the deviation of the channel diameters from the nominal values given by the manufacturer, and to the different efficiencies of the four filter papers as second-sound transducers. This will be discussed in more detail in Sec. IV B.

We have normalized the mean values for $d\rho_{s,0}/T$ from the four filter papers (using the factors 1.27, 0.92, 1.03, 0.87 for the 0.1-, 0.2-, 0.4-, 0.6-μm papers, respectively) to get an over-all mean value of $10^8 \, d\rho_{s,0}/T = 0.668$. The resulting values are plotted in Fig. 16 with higher resolution than was possible in Fig. 15. Our data are in agreement with

$$\xi \rho_s / T = \text{const} \pm 2\% \tag{16}$$

for all pressures along the λ line. As stated earlier for the validity of Eq. (9), the slight trend of some of the data is within the uncertainty of our data and does not allow us to establish a pressure dependence for $\xi\rho_s/T$ outside of the errors. The correlation length which satisfies Eq. (15) is the phase-coherence length according to the derivation of Eq. (15) in Refs. 10 and 11. Our result $d\rho_s/T$ = const demonstrates, therefore, that the phase-coherence length and the onset length in ^{4}He are related by a constant multiplicative factor.

Since our data are taken as a function of pressure at constant d or ξ, the above result for $\xi\rho_s/T$ means that for all pressures and at constant ϵ along the λ line,

$$\rho_s/T = \text{const} \pm 2\%.$$

This result was checked explicitly by calculating ρ_s/T for different ϵ within the range $2\times10^{-5} \lesssim \epsilon \lesssim 2\times10^{-4}$ as a function of P from the original data of Greywall and Ahlers.[4] Indeed, this calculation verified that ρ_s/T is independent of pressure to better than 2% for the above range of ϵ! We do not know what this close relation between ρ_s (near T_λ) and T_λ both as a function of P means, and are not aware of any corresponding prediction.

Recently Ikushima and Terui[29] have determined ξ at several pressures from their measured values of ρ_s assuming the validity of Eq. (15) and a pure power law for ρ_s/ρ. They find the correlation length ξ to be proportional to the interatomic distance a, and find that ξ^*/a is a constant to within about 2%. The interatomic distance decreases

by about 7% along the λ line. Therefore, their result implies that ξ^* decreases by about $(7\pm2)\%$ from SVP to the melting curve. Our results for the correlation length show that ξ^* is a constant to within 2% along the λ line [if we fix the exponent $\nu'(P) = \text{const}$]. Any relation between ξ and a is somewhat surprising, because the order parameter does not couple to the total density of the liquid.

We discussed in Sec. III C 3 that the choice of the cutoff voltage level for the vanishing of second sound used in the data analysis has no influence on the pressure dependence of our result. Its small influence on the absolute values is explicitly shown for the quantity $d\rho_{s,0}/T$ in Figs. 17 and 18. The lower set of data points in Fig. 18 was discussed above, and results from an analysis using a cutoff level for the second-sound amplitude of 0.1 μV. The upper set of data points comes from exactly the same analysis except using a cutoff level of 1 μV. It is clear that the general trend of the data points, their scatter, and the extent to which they show no dependence on pressure have not been altered by this factor-of-10 change in the cutoff level used. In addition, the absolute value of $d\rho_{s,0}/T$ is only changed by 22% due to this 1000% change in the cutoff level. This example is indicative of the cutoff voltage dependence for the absolute value of all the quantities determined from our data, and will be discussed in more detail in Sec. IV B. Therefore, any foreseeable reduction of the noise level of the apparatus (and hence the cutoff level) would produce a very small change in the absolute values quoted in our results,
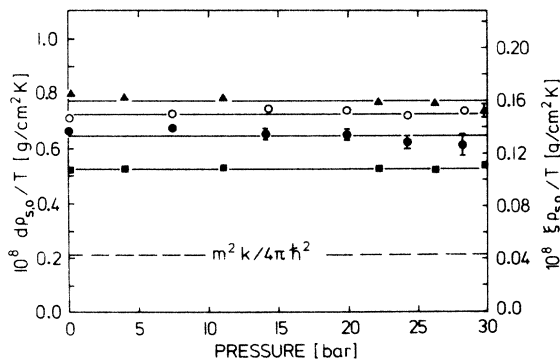

FIG. 15. Scaling quantity $d\rho_{s,0}/T$ as a function of pressure for four filter papers: ▲, $d=0.6$ μm; ●, $d=0.4$ μm; ○, $d=0.2$ μm; ■, $d=0.1$ μm. ($\rho_{s,0}$ is the superfluid density at the onset temperature T_0.) The right-hand scale gives the same quantity with d replaced by the correlation length using the Ginzburg-Pitaevskii-Mamaladze relation $\xi = 0.207$ d (Ref. 8). Also shown is the value of the constant $\xi\rho_s/T$ predicted in Refs. 10 and 11, whose absolute value refers to the right-hand scale. Error bars are shown only when they are larger than the data point.
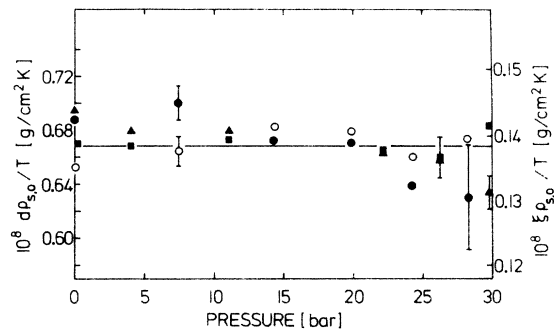

FIG. 16. Scaling quantity $d\rho_{s,0}/T$ as a function of pressure for four filter papers with channel diameter $d = 0.6$ μm (▲); 0.4 μm (●); 0.2 μm (○); 0.1 μm (■). ($\rho_{s,0}$ is the superfluid density at the onset temperature T_0). The right-hand scale gives the same quantity with d replaced by the correlation length ξ using the Ginzburg-Pitaevskii-Mamaladze relation $\xi = 0.207$ d (Ref. 8). The data shown are obtained from the data of Fig. 15 or Table II by normalizing them to their over-all mean value for all filter papers. Some representative error bars are shown.

and would not affect at all the pressure indepen-
dences we have determined.

B. Absolute values

To obtain absolute values for λ', ν', d^*, and ξ^*,
we have to compare data from different filter
papers. We encounter two problems in this analy-
sis: The absolute values for the channel diameters
d have to be known, as well as which part of their
size distribution is determining our results. For
the values and distribution of the channel sizes we
take the information from the manufacturer,[24]
which is given in Table I. We guess that the very
weak sound signals we see near the cutoff level are
generated preferentially by the channels at the
large-diameter tail of the channel size distribution,
which are left "open" at temperatures where
smaller channels are already "plugged" for the
superfluid component of liquid helium. According
to the information from the manufacturer for the
0.2-, 0.4-, and 0.6-μm paper, the values at the
upper-tail end in the size distribution are these
nominal values and the papers should "contain no
channels larger than these values."[24] We there-
fore used the nominal values for the channel
diameters d to deduce the absolute values for the
various quantities to be discussed below.

A more serious problem for the analysis of
data taken with different filter papers is the differ-
ent efficiency of the four papers for the genera-
tion or detection of second sound. In Table I we
show that using the same drive voltage of 0.68 V_{rms}
gave second-sound signals between 0.3 and 8 mV
at temperatures clearly below T_0. Because of the
varying transducer efficiency it might have been
more meaningful for the determination of absolute
values from different filter papers to take the data
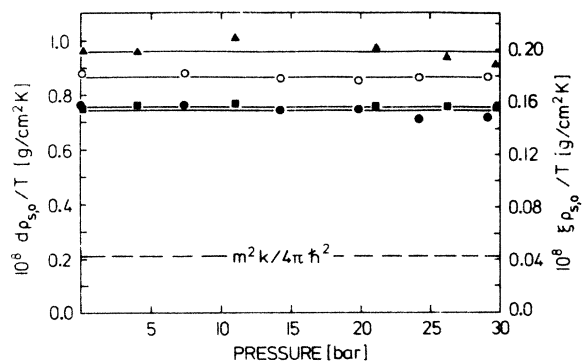not with a constant drive voltage but with a con-

stant signal at a temperature clearly below T_0.
We have discussed in Sec. III C 2 how the values
for second-sound velocity or onset temperature
are changed by changing the drive signal (see Fig.
11). A one-to-one relation between a change in
transducer efficiency and a change in drive voltage
may, of course, not be quite correct, but this
comparison should enable us to determine approx-
imately the changes introduced due to different
signal sizes. To take the varying amplitudes into
account, we have normalized our data to the data
taken with the 0.6-μm paper which gave the
weakest signals. For this paper we left the cutoff
level at our noise level of 0.1 μV (see Sec. III A).
The cutoff levels for the other three papers were
increased proportional to their signals A_d at
temperatures clearly below T_0; the cutoff level is
0.1 μV$\times(A_d/A_{0.6\,\mu m})$ (A_d from Table I). An error
introduced by this shift in cutoff level may be the
fact that at the higher amplitudes the second-sound
signal should be determined by another part in the
channel size distribution than it was at the 0.1-μV
level. For that reason we take the full range for
the channel sizes d ($\pm 10\%$) given by the manu-
facturer as the error for d.

As an example for the change in the data intro-
duced by this change in cutoff level, we show in
Fig. 19 the data for the reduced cutoff temperature
$\epsilon_{0,c}$ determined by this analysis. We emphasize
that the changes in cutoff level which are quite
drastic for the 0.2- and for the 0.1-μm paper, do
not change the general behavior of the data and
especially do not influence their pressure inde-
pendence. With the adjusted cutoff levels we get

FIG. 17. As in Fig. 15, but with the cutoff level for
the sound taken at 1.0 μV instead of 0.1 μV. The pres-
sure independence of the scaling quantity is not influenced
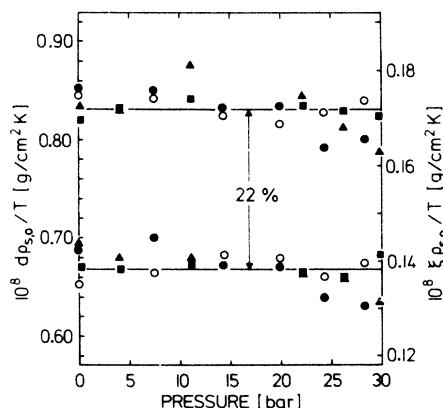by this drastic change in cutoff level.

FIG. 18. Same as Fig. 16. The lower set of data is
identical to the data of Fig. 16 and shows the results if
we determine them from the cutoff level for the second
sound at 0.1 μV. The upper set of data would result if
we shift the cutoff level by an order of magnitude to 1.0
μV. The scaling quantity $\xi\rho_s/T$ is still constant, and
its absolute value is increased by only 22%.

as mean values $10^6 \epsilon_{0,c} = 335$, 134.7, 34.5, and 23.0 for the 0.1-, 0.2-, 0.4-, and 0.6-μm papers, respectively, instead of the values given in Table II.

Using these values, we can extend the previously known data for the onset temperature as a function of the dimension d in superfluid helium by about an order of magnitude to higher d and smaller ϵ. They are in good agreement with the data for smaller dimensions, as collected in Fig. 30 of Ref. 1 for example, and therefore support ϵ_0 $\propto d^{-3/2}$.

Taking the above data for $\epsilon_{0,c}$ and d we have performed a two-parameter (λ', d^*) least-squares fit resulting in

$$\epsilon_{0,c} = (d/d^*)^{-1.54 \pm 0.05},$$

with $d^* = (5.7 \pm 0.6) \times 10^{-8}$ cm.

And with Eq. (14) we find for the correlation length

$$\xi = (1.2 \pm 0.1) \times 10^{-8} \epsilon^{-0.65 \pm 0.02} \text{ cm}.$$

For this fit the data were weighted by the factors 7, 6, 2, and 5 for the 0.1-, 0.2-, 0.4-, and 0.6-μm papers, respectively, according to the accuracy of the data from the four runs. The quoted errors result from the uncertainties for the channel diameters d.

The scaling laws[5,30] $\zeta = \nu'$ and $3\nu' = 2 - \alpha'$ (which pertains to a three-dimensional system), together
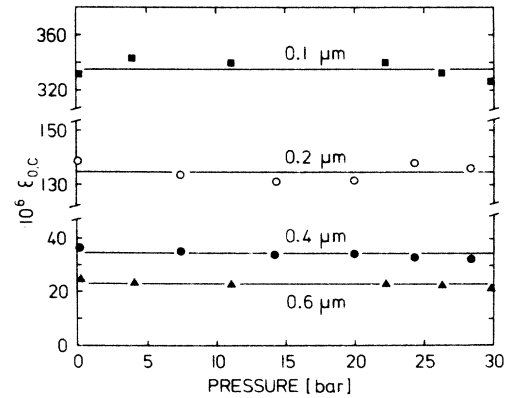

FIG. 19. Reduced temperature difference $\epsilon_{0,c}$ as a function of pressure. $\epsilon_{0,c}$ was determined from the velocity of second sound at amplitudes of 0.1, 0.2, 0.77, and 2.67 μV for the 0.6-μm (▲), 0.4-μm (●), 0.2-μm (○), and 0.1-μm (■) filter papers, respectively. The change in cutoff level does not change the pressure independence of $\epsilon_{0,c}$. Horizontal lines are drawn through the average values of $\epsilon_{0,c}$ for each filter paper. Note the discontinuous vertical scale.

with the experimental results for the exponent describing the singularity in the heat capacity $(\alpha' = -0.01 \pm 0.03)$,[6] and for the exponent of ρ_s/ρ $(\zeta = 0.67 \pm 0.01)$,[4] yield at all pressures $\nu' = 0.67$ ± 0.01. This number is in agreement with our above results. Our results for ν' are also in

TABLE III. Determinations of the correlation length for the superfluid state. Only in Refs. d and e, and in this experiment, was the exponent ν' treated as a free variable and not assumed to be $\frac{2}{3}$; the data of Ref. 33 is for $P = 25.1$ atm; all other data besides ours were taken at SVP.

System	Method	ξ (Å)	Ref.
Bulk	Attenuation first sound	(1.2 and 2.4) $\epsilon^{-2/3}$	a
Bulk	Attenuation first sound	0.81 $\epsilon^{-2/3}$	b
Bulk	Intensity first sound/second sound	2.0 ± 0.4 $\epsilon^{-2/3}$	33
Channels	Vanishing of second sound	1.2 ± 0.1 $\epsilon^{-0.65 \pm 0.02}$	This work
Pores	Fourth sound	$1.8^{+5.6}_{-1.5} \epsilon^{-0.75 \pm 0.07}$	c
Pores	Persistent current; Gravitational flow	2.8 ± 0.35 $\epsilon^{-0.67 \pm 0.04}$	d
Film	Third sound	1.8 $\epsilon^{-2/3}$	12
Film	Heat transport	1.6 $\epsilon^{-2/3}$	13
Bulk	Theory	0.3 $\epsilon^{-2/3}$	10, 11
Bulk	Theory	1.2 $\epsilon^{-2/3}$	e
Boundary	Theory	1.63 $\epsilon^{-2/3}$	8

[a] G. Ahlers, J. Low Temp. Phys. 1, 609 (1969).

[b] R.D. Williams and I. Rudnick, Phys. Rev. Lett. 25, 276 (1970), but see Ref. 26.

[c] M. Kriss and I. Rudnick, J. Low Temp. Phys. 3, 339 (1970).

[d] R. P. Henkel, E. N. Smith, and J. D. Reppy, Phys. Rev. Lett. 23, 1276 (1969); an improved analysis of the data gave $\nu' = 0.63 \pm 0.05$ [R.P. Henkel, thesis (Cornell University, 1970) (unpublished)].

[e] J.A. Tyson, in *Proceedings of the International Conference on Fluctuations in Superconductors, Asilomar, Calif.*, edited by W. S. Goree and F. Chilton (Stanford Research Institute, Menlo Park, Calif., 1968), p. 343; M.E. Fisher, *ibid*, p. 357.

agreement with phenomenological calculations of ξ, as shown in Table III. The absolute value we find for ξ^* is about 30% smaller than the value from the GPM theory,[8] but almost a factor of 4 larger than the correlation length defined in Ref. 10 and 11. Because of the uncertainties about numerical factors in these calculations,[8,10,11,31] we do not consider the apparent disagreement with the predictions significant.

There are two groups of experiments by which a characteristic length for the superfluid state has been measured at SVP for the temperature range $\epsilon < 10^{-1}$: (i) acoustic experiments in bulk He II; and (ii) depletion of ρ_s in restricted geometries. Their results are summarized in Table III. The summarized experimental results show values for ξ^* ranging from 0.8 to 2.8 Å. The experiments are distinguished by the system (bulk, films, helium in pores or channels), the substrate for the experiments in restricted geometries, and last but not least the experimental method. Considering these differences, we find the agreement between the data, demonstrated in Table III, remarkable. We believe that the geometry for our experiment is known at least as well as for any other experiment performed in restricted geometries. The only experiment performed at a higher than saturated vapor pressure gave a value of $\xi^* = 2.0 \pm 0.4$ Å at $p = 25.1$ atm, assuming an exponent of $\nu' = \frac{2}{3}$.[33] Taking into account the very different method and theory to extract this value for ξ^* from the data of Ref. 33, we feel that it is in agreement with our result that the pressure has no or very little influence on the correlation length.

From the analysis with different cutoff levels we find $10^8 d\rho_{s,0}/T = 0.789$, 0.850, 0.676, and 0.772 g/cm^{2}K for the 0.1-, 0.2-, 0.4-, and 0.6-μm papers, respectively, instead of the values given in Table II. The scatter of these values is within the $\pm 10\%$ uncertainty of the channel diameter d. The mean of these four values is

$$10^8 d\rho_{s,0}/T = 0.77 \pm 0.04 \text{ g/cm}^2\text{K},$$

and gives with Eq. (14)

$$10^8 \xi\rho_{s,0}/T = 0.16 \pm 0.01 \text{ g/cm}^2\text{K}.$$

(If we weight the results from the four filter papers by 7, 6, 2, and 5 as we did for determining λ' and d^*, we find 0.79 and 0.16 for the above two quantities, respectively.) Both values are only about 15% larger than the results from the analysis with a constant cutoff level of 0.1 μV (0.67 and 0.14 g/cm^{2}K, respectively), which represent a lower limit. The somewhat low value from the data with the 0.4-μm paper may result from the

lower accuracy of this run. We compare our results to theoretical predictions and experiments performed at SVP. The mean value for $\xi\rho_s/T$ is smaller than calculated for SVP from phenomenological GPM theory (0.263),[8] but larger than predicted in Ref. 10 and 11 (0.044). As mentioned above, we do not consider this disagreement to be significant because of the uncertainties about numerical factors in these calculations. The quantity $\xi\rho_s/T$ has been determined as a function of temperature at SVP in two other experiments, giving the following values:

$$10^8 \xi\rho_s/T = 0.289 \text{ for } 1.125 < T < 2.046 \text{ (Ref. 12)},$$

$$= 0.264 \text{ for } 1.37 < T < 2.13 \text{ (Ref. 13)}.$$

These values are very close to GPM value.[8] Both results are from film experiments and assume ρ_s to vanish at the solid and at the free boundary.[34] The above two numbers for $\xi\rho_s/T$ have been determined on quite different systems with very different methods compared to ours. These facts, an uncertainty about the film thickness (at least for Ref. 12), or about the boundary condition at the free surface, may be responsible for the difference between the above numbers and our result.

V. SUMMARY AND CONCLUSIONS

We have determined the onset temperature for superfluidity of ^{4}He by observing the vanishing of second sound in resonators equipped with superleak transducers. The experiments have been performed between saturated vapor pressure and the melting curve of ^{4}He. A precise pressure-regulating system has been developed for these experiments. The onset temperatures $T_0(P)$ in the investigated channels ($d = 0.1$, 0.2, 0.4, and 0.6 μm) were in the range $2 \times 10^{-5} \lesssim \epsilon_0 = 1$ $- T_0(P)/T_\lambda(P) \lesssim 2 \times 10^{-4}$. We find that the reduced shift ϵ_0 of the onset temperature, the quantities $\xi\rho_s/T$ and ρ_s/T, as well as the exponents and coefficients for the equations $\epsilon_0 = (d/d^*)^{-\lambda'}$ and $\xi = \xi^* \epsilon^{-\nu'}$ are, within our errors, independent of pressure (ξ is the correlation length). The quantity $\xi\rho_s/T$ is constant over a very wide temperature range at SVP,[12,13] and for all pressures along the λ line. The appreciable temperature and pressure dependences of ξ, ρ_s, and $T_\lambda(P)$ have to cancel each other. The absence of a pressure dependence of the exponents λ' and ν' is in agreement with the universality concept for the superfluid phase of liquid helium.[3] Our results support Ahlers'[1,4] suggestion that the observed deviations from universality and scaling are likely to result from properties in the normal fluid phase of liquid

helium. For the absolute values we find

$$\xi = (1.2 \pm 0.1) \times 10^{-8} \, \epsilon^{-0.65 \pm 0.02}, \quad \epsilon_0 = [d/(5.7 \pm 0.6) \times 10^{-8}]^{-1.54 \pm 0.05}, \quad \xi \rho_s/T = (0.16 \pm 0.01) \times 10^{-8}.$$

ACKNOWLEDGMENTS

*Present address: Dept. of Physics, Ohio State University, Columbus, Ohio 43210.

[1] G. Ahlers, in *The Physics of Liquid and Solid Helium*, edited by K. H. Bennemann and J. B. Ketterson (Wiley, New York, to be published), Chap. 5, Vol. I.

[2] K. G. Wilson and M. E. Fisher, Phys. Rev. Lett. 28, 240 (1972); K. G. Wilson, Phys. Rev. Lett. 28, 548 (1972); E. Brézin, D. J. Wallace, and K. G. Wilson, Phys. Rev. Lett. 29, 591 (1972); Phys. Rev. B 7, 232 (1973).

[3] L. P. Kadanoff, in *Proceedings of the International School of Physics "Enrico Fermi,"* Course LI, edited by M. S. Green (Academic, New York, 1971); R. B. Griffiths, Phys. Rev. Lett. 24, 1479 (1970).

[4] D. S. Greywall and G. Ahlers, Phys. Rev. Lett. 28, 1251 (1972); Phys. Rev. A 7, 2145 (1973).

[5] B. D. Josephson, Phys. Lett. A 21, 608 (1966).

[6] G. Ahlers, Phys. Rev. A 8, 530 (1973).

[7] R. Williams, S. E. A. Beaver, J. C. Fraser, R. S. Kagiwada, and I. Rudnick, Phys. Lett. A 29, 279 (1969); R. A. Sherlock and D. O. Edwards, Rev. Sci. Instrum. 41, 1603 (1970).

[8] V. L. Ginzburg and L. P. Pitaevskii, Zh. Eksp. Teor. Fiz. 34, 1240 (1958) [Sov. Phys.-JETP 7, 858 (1958)]; Yu. G. Mamaladze, Zh. Eksp. Teor. Fiz. 52, 729 (1967) [Sov. Phys.-JETP 25, 479 (1967)].

[9] A. E. Ferdinand and M. E. Fisher, Phys. Rev. 185, 832 (1969); M. A. Moore, Phys. Lett. A 37, 345 (1971); M. E. Fisher and M. N. Barber, Phys. Rev. Lett. 28, 1516 (1972).

[10] R. A. Ferrell, N. Menyhárd, H. Schmidt, F. Schwabl, and P. Szépfalusy, Ann. Phys. (N.Y.) 47, 565 (1968).

[11] B. I. Halperin and P. C. Hohenberg, Phys. Rev. Lett. 19, 700 (1967); Phys. Rev. 177, 952 (1969).

[12] I. Rudnick and J. C. Fraser, J. Low Temp. Phys. 3, 225 (1970).

[13] E. S. Sabisky and C. H. Anderson, Phys. Rev. Lett. 30, 1122 (1973); and private communication.

[14] G. C. Straty and E. D. Adams, Rev. Sci. Instrum. 40, 1393 (1969).

[15] Model CMM, Heise Bourdon Tube Co., Newton, Conn. The accuracy of the gauge given by the manufacturer is ±0.03 bar. The calibration of the gauge was checked with a dead-weight tester. It was found that the scale on the gauge had to be adjusted by a factor of 0.996.

For the upper λ temperature and λ pressure we measured $T_\lambda = 1.762 \pm 0.001$ K and $P_\lambda = 29.74 \pm 0.03$ bar. These values are in agreement with the most recent values 1.7633 ± 0.0001, 29.74 ± 0.05 from Kierstead (Ref. 16).

[16] H. A. Kierstead, Phys. Rev. 162, 153 (1967).

[17] Model 1615-A, General Radio Comp., Concorde, Mass.

[18] Ultraminiature coaxial cable, Lake Shore Cryotronics, Eden, N. Y.

[19] G. Ahlers and F. Pobell (unpublished).

[20] Model CR 2500 L, Cryo Cal Inc., Riviera Beach, Florida.

[21] Barocell 511-11, CGS Datametrics, Watertown, Mass.

[22] Model 1900-A, General Radio Comp., Concorde, Mass.

[23] G. Ahlers, Phys. Rev. 171, 275 (1968).

[24] Nuclepore Corporation, 7035 Commerce Circle, Pleasanton, Calif. Information was supplied by Dr. S. C. Furman, who offers samples to other workers.

[25] G. Ahlers, Phys. Rev. 182, 352 (1969).

[26] W. C. Thomlinson and F. Pobell, Phys. Rev. Lett. 31, 283 (1973).

[27] J. R. Clow and J. D. Reppy, Phys. Rev. Lett. 19, 291 (1967).

[2b] Although the linearity of u_2 in P is not obvious from Eq. (5) of Ref. 4, the data quoted there can be represented in a form which shows that deviations from this linearity are of order 2% or less for the pressure and temperature range of our experiment.

[29] G. Terui and A. Ikushima, Phys. Lett. A 39, 161 (1972); A. Ikushima and G. Terui, J. Low Temp. Phys. 10, 397 (1973).

[30] B. Widom, J. Chem. Phys. 43, 3892 (1965); J. Chem. Phys. 43, 3898 (1965); L. P. Kadanoff, Physics 2, 263 (1966); R. B. Griffiths, Phys. Rev. 158, 176 (1967).

[31] K. Binder and P. C. Hohenberg, Phys. Rev. B 6, 3461 (1972); P. C. Hohenberg, J. Low Temp. Phys. (to be published).

[32] I. M. Khalatnikov, *Introduction to the Theory of Superfluidity* (Benjamin, New York, 1965).

[33] G. Winterling, F. S. Holmes, and T. J. Greytak, Phys. Rev. Lett. 30, 427 (1973).

[34] The determination of the thickness of an immobile layer at the substrate and of the proportionality between onset thickness l and correlation length ξ are slightly different in Ref. 12 ($l = 2\sqrt{2}\,\xi$), and Ref. 13 ($l = \pi\xi$).